

A Comparison of the Krawinkler and Scissors Models for Including Beam-Column Joint Deformations in the Analysis of Moment-Resisting Steel Frames

FINLEY A. CHARNEY and JUSTIN MARSHALL

The significance of beam-column joint deformations on the overall flexibility of steel moment resisting frames has been known for some time (Bertero, Popov, and Krawinkler, 1972; Becker, 1975). This is true for elastic response and particularly for inelastic response when shear yielding occurs in the panel zone region of the joint. Structural analysis should always include such deformations. This point is clearly stated in the latest design provisions for seismic analysis and design of structures (ASCE, 2002; FEMA, 2000; FEMA, 2004). Unfortunately, these provisions provide no explicit recommendations for mathematical modeling of the joint, even when the joint remains elastic.

Other design documents provide ambiguous or even misleading guidance. For example, FEMA 356 (FEMA, 2000c), states that panel zone flexibility may be modeled by adding a panel zone element to the mathematical model or by adjusting the beam flexural stiffness. Again, no details are provided on how a panel zone element would be used. Furthermore, the notion that the beam flexural stiffness may be altered to represent inelastic panel zone behavior is fundamentally incorrect.

FEMA 355C (FEMA, 2000a) recommends the use of two different joint models, known as the Krawinkler model (Krawinkler, 1978), and the Scissors model. Each model is based on simple mechanical analogs consisting of assemblages of rigid links and rotational springs. FEMA 355C does not provide detailed information on the use of these models. In fact, very few of the reference articles that describe these models provide specific information on how the mechanical properties that control the models (for example, moment rotation relationships for the springs) are to be computed.

A far more serious problem is that several articles that refer to both the Krawinkler and Scissors models incorrectly suggest that the spring properties derived for the Krawinkler model may be used directly in the Scissors model. For example, FEMA 355F (2000b) has an illustration (Figure 4.7 in that document) with an arrow that points to a spring in the Scissors model and provides an equation for the spring stiffness that is applicable *only* to the Krawinkler model. A more recent example is a paper by Castro, Elghazouli, and Izzuddin (2005) that clearly suggests that the properties are interchangeable.

The erroneous notion that the properties for the Krawinkler model may be used in the Scissors model is based on the assumption that, under a given loading, the rotation in the spring of the Scissors model is the same as the shear strain in the panel of the Krawinkler model. As illustrated in this paper, this assumption fails to recognize the significant differences in the geometry and kinematics of the two models.

The purpose of this paper is to remove the ambiguities and misunderstandings that lead to the misuse of the Krawinkler and Scissors models. This is done by providing detailed derivations of the mechanical properties of the models and by demonstrating their use in the analysis of a simple moment resisting frame. Through this example, it is shown that the results obtained from the Krawinkler and Scissors models are very similar for elastic response but that significant differences may occur when ductility demands are high. It is also shown unequivocally that very significant errors are obtained when the Krawinkler spring properties are used in the Scissors model. The errors generally cause a significant underestimate of system strength and stiffness, which will have a negative impact on the economy of steel moment frames.

NOMENCLATURE

A typical interior beam-column subassemblage of a moment-resisting steel frame is shown in Figure 1. In the figure, H represents the story-to-story column height, and L is the width of a typical bay. The shear force acting on the columns, V_c , is the average of the actual shears in the columns above and below the joint. The subassemblage is in equilibrium under the loads shown if the moments at the mid-span of the beams and mid-height of the columns are

Finley A. Charney is associate professor, department of civil and environmental engineering, Virginia Tech, Blacksburg, Virginia.

Justin Marshall is a graduate student, department of civil and environmental engineering, Virginia Tech, Blacksburg, Virginia.

zero. This has been enforced in the subassembly by inserting real hinges at mid-height of the columns above and below the joint and by inserting hinges at mid-span of the beams on either side of the joint.

It is assumed that the size and span of the beams on either side of the column are the same and that a single column section is used over the full height. The column runs through the joint, and the beams are welded to the column flanges. A doubler plate may be used to reinforce the panel zone. If used, the doubler plate is assumed to act integrally with the column web and to have the same yield strength as the web.

The terms α and β in Figure 1 represent the ratios of the effective depth of the column to the span length and the effective depth of the beam to the column height, respectively. In this paper, the effective depth of a section is defined as the distance between the center of the flanges. Thus

$$\alpha = \frac{d_c - t_{fc}}{L} \quad (1)$$

$$\beta = \frac{d_b - t_{fb}}{H} \quad (2)$$

where d_c and d_b are the depths and t_{fc} and t_{fb} are the flange thicknesses of the columns and beams, respectively. The use of the terms α and β in lieu of the actual physical dimensions of the sections greatly simplifies the derivation of the model's properties.

TOTAL SUBASSEMBLAGE DRIFT

The total drift in the subassembly, Δ , is defined as the lateral displacement of the top of the upper half-column with respect to the bottom of the lower half-column under the applied load V_c . This drift is shown in Figure 2.

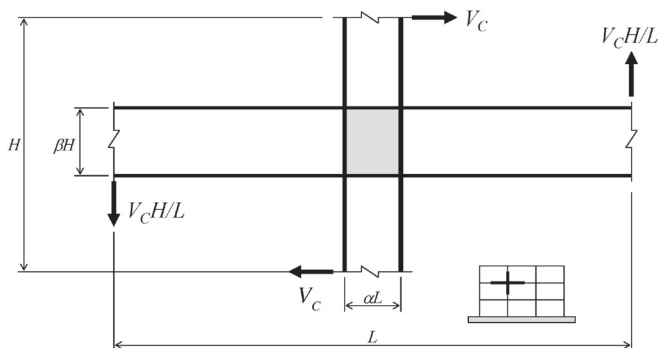


Fig. 1. Typical interior beam-column subassembly.

Following the procedure described by Charney (1993), this drift may be divided into three components, one for the column region outside the joint, one for the beam region outside the joint, and one for the beam-column joint itself:

$$\Delta = \Delta_c + \Delta_b + \Delta_j \quad (3)$$

In Equation 3, each of the individual drift components may arise from elastic or inelastic deformations. P-Delta effects may be included separately, as necessary. This paper concentrates on the development of the joint deformation term only. This term may be further subdivided into three components, also representing axial, flexural, and shear deformation:

$$\Delta_j = \Delta_{jA} + \Delta_{jF} + \Delta_{jV} \quad (4)$$

The axial deformation term, Δ_{jA} , is not considered in this paper. This source of deformation is almost always elastic and is negligible for frames with about 10 stories or less (Charney, 1990). The flexural joint deformation term, Δ_{jF} is also elastic and is due to normal stresses resulting from bending that occurs through the width and depth of the joint. This is a source of flexibility in the joint and should not be confused with the column flange bending component of resistance (described later), which is treated as a source of stiffness. The flexibility associated with bending in the panel is generally not included in the Krawinkler and Scissors models and is not considered further herein. It is noted, however, that preliminary recommendations for including flexural deformations are presented in Downs (2002).

THE ORIGINAL KRAWINKLER MODEL

If it is assumed that the moment in the beam at the face of the column is resisted entirely by the flanges of the beam, it can be shown by simple statics that the horizontal shear force in

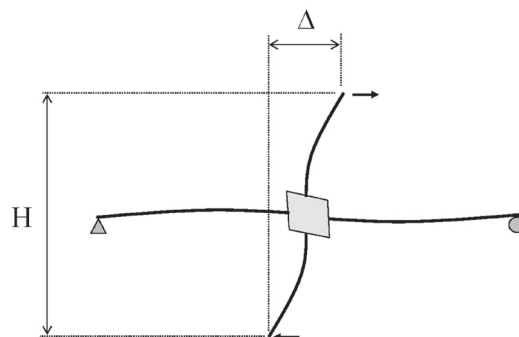


Fig. 2. Drift in typical subassembly.

the beam-column joint is

$$V_J = \frac{V_C(1-\alpha-\beta)}{\beta} \quad (5)$$

According to Krawinkler (1978) this shear is resisted by shear in the panel zone, V_p , and by shear in the column flanges, V_f , on either side of the panel:

$$V_J = V_p + V_f \quad (6)$$

In Krawinkler's original model, shown in Figure 3, the panel shear is resisted by an elastic-plastic membrane element, and the flange shear is resisted by four rotational springs, each situated at a different corner of a linkage of four rigid bars.¹ The beams and columns frame into the linkages at right angles. A total of 12 nodes are required for the model (there are two nodes at each corner). The number of degrees of freedom (DOF) in the model depends on the use of nodal constraints or slaving. The minimum number

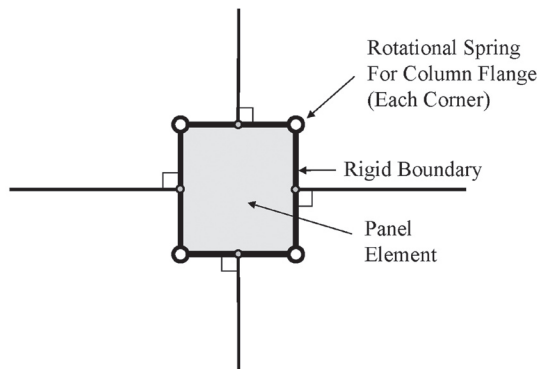


Fig. 3. The original Krawinkler beam-column joint model.

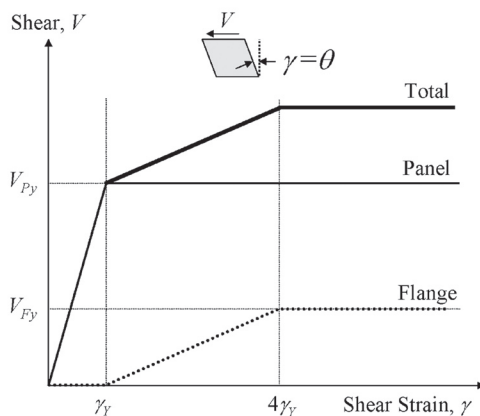


Fig. 4. Force deformation relationship for the original Krawinkler model.

of DOF required to model the panel is four in a planar structure. The maximum is 28.

The assumed force-deformation behavior of each component of the model is shown in Figure 4. This behavior is identical to that assumed by Krawinkler (1978). Note that Figure 4 is presented in terms of shear force on the vertical axis and shear strain on the horizontal axis. As indicated in the inset to Figure 4, rotations in the flange springs, θ , are synonymous with shear strains in the panel, γ .

Note from Figure 4 that the elastic-plastic panel component resists shear force immediately, but the flange component is assumed to provide no resistance until the panel yields. The flange component eventually yields at 4.0 times the yield strain of the panel component. Strain hardening may be included by providing some positive post-yield stiffness in either component of the model.

Assuming the steel yields in shear² at $F_y/\sqrt{3} \approx 0.6 F_y$ and that the column and doubler are made of the same material, the yield strength of the panel is

$$V_{Py} = 0.6 F_y \alpha L t_p \quad (7)$$

where t_p is the thickness of the column web, plus the doubler plate thickness, if present. The corresponding yield strain is

$$\gamma_y = \frac{0.6 F_y}{G} \quad (8)$$

where G is the shear modulus of the steel. The initial shear stiffness of the panel component of resistance is

$$K_{P\gamma} = \frac{V_{Py}}{\gamma_y} = G \alpha L t_p \quad (9)$$

Krawinkler (1978) gives the initial rotational stiffness for each of the four flange springs as

$$K_{F\theta} = \frac{M_F}{\theta} = \frac{E(b_{fC})(t_{fC})^2}{10} = 0.26 G(b_{fC})(t_{fC})^2 \quad (10)$$

where b_{fC} and t_{fC} are the width and thickness, respectively, of the flanges of the column, and the shear modulus G is taken as $E/2.6$. The flange shear is related to the moment as follows:

¹ If the rigid link is to be modeled using frame elements, its axial area and moment of inertia should be on the order of 1,000 times that of the largest beam or column of the structure. Use of properties greater than this may lead to loss of accuracy in the solution of the equilibrium equations (Bathe, 1996).

² Note that Krawinkler's original paper uses $0.55 F_y$ for the yield stress in shear.

Table 1. Summary of Properties for Original Krawinkler Model Using Original Force-Deformation Model				
Component	Spring Type	No. of Springs	Spring Stiffness	Spring Strength
Panel	Membrane	1	$K_{PK} = G \alpha L t_p$	$V_{PK} = 0.6 F_y \alpha L t_p$
Flanges	Rotational	4	$K_{FK} = 0.26 G (b_{fC})(t_{fC})^2$	$M_{FK} = 0.468 F_y (b_{fC})(t_{fC})^2$
See Figure 3 for illustration of model See Figure 4 for force-deformation relationships				

$$V_F = \frac{4M_F}{\beta H} \quad (11)$$

Dividing the left side of Equation 11 by γ and the right side by θ produces

$$\frac{V_F}{\gamma} = \frac{4}{\beta H} \frac{M_F}{\theta} \quad (12)$$

Recognizing the left term as the total flange shear stiffness, and substituting from Equation 10 on the right

$$K_{F\gamma} = \frac{1.04G(b_{fC})(t_{fC})^2}{\beta H} \quad (13)$$

The γ in the subscript on K is a reminder that $K_{F\gamma}$ is a shear stiffness, as opposed to a rotational stiffness, which was designated with a θ in the subscript in Equation 10. The total flange shear at yield is based on Figure 4 where it is seen that

$$V_{Fy} = K_{F\gamma}(3\gamma_y) \quad (14)$$

Substituting Equation 13 for the flange stiffness, and using Equation 8 for the yield strain, the total flange strength is

$$V_{Fy} = 1.87 \frac{F_y (b_{fC})(t_{fC})^2}{\beta H} \quad (15)$$

Using Equations 11 and 15, the rotational strength of each of the four flange springs is simply

$$M_{Fy} = \frac{V_{Fy}\beta H}{4} = 0.468 F_y (b_{fC})(t_{fC})^2 \quad (16)$$

The four required properties for the original Krawinkler model are summarized in Table 1.

It is important to note that the flange shear strength given by Equation 16 is significantly greater than would be obtained from the flexural strength of the flanges alone. This

can be demonstrated by application of a virtual unit strain in the panel, which results in a displacement of βH at the top of the panel with respect to the bottom of the panel. The external virtual work done by the "ultimate" shear force V_{Fu} moving through this displacement is $V_{Fu}(\beta H)$. The plastic rotation in a single flange spring is 1.0, and the moment capacity of the spring is equal to the plastic moment capacity of the flange, or $(b_{fC})(t_{fC})^2 F_y / 4$. The internal work in four such springs is $(b_{fC})(t_{fC})^2 F_y$. Equating internal and external work gives

$$V_{Fu} = \frac{(b_{fC})(t_{fC})^2 F_y}{\beta H} \quad (17)$$

which is substantially less than (by a factor of 1.87) that given by Equation 15. Equation 15 is favored for the flange component because it correlates well with experimental results (Krawinkler, 1978).

Before continuing, it is of interest to compare the strength of the joint provided by the Krawinkler model with the strength, which would be computed by the current design provisions. The maximum shear resistance for the entire Krawinkler joint is equal to the strength of the panel component plus the strength of the flange component. Using Equations 7 and 15,

$$V_{Jy} = V_{Py} + V_{Fy} = 0.6 F_y \alpha L t_p + 1.87 \frac{(b_{fC})(t_{fC})^2 F_y}{\beta H} \quad (18a)$$

which may be reorganized as follows:

$$V_{Jy} = 0.6 F_y \alpha L t_p \left[1 + 3.12 \frac{(b_{fC})(t_{fC})^2}{\alpha L \beta H t_p} \right] \quad (18b)$$

Equation 18b is very similar to that provided by the AISC Specification (AISC, 2005) and the AISC Seismic Provisions for Structural Steel Buildings (AISC, 2005):

$$R_v = 0.6 F_y d_c t_p \left[1 + 3.00 \frac{(b_{fC})(t_{fC})^2}{d_B d_c t_p} \right] \quad (19)$$

Table 2. Summary of Properties for Revised Krawinkler Model Using Original Force-Deformation Relationships				
Component	Spring Type	No. of Springs	Spring Stiffness	Spring Strength
Panel	Rotational	1	$\bar{K}_{PK} = G\nabla_P$	$\bar{M}_{PK} = 0.6 F_y \nabla_P$
Flanges	Rotational	1	$\bar{K}_{FK} = 1.04 G (b_{fC})(t_{fC})^2$	$\bar{M}_{FK} = 1.87 F_y (b_{fC})(t_{fC})^2$
See Figure 5 for illustration of model See Figure 4 for force-deformation relationships				

Aside from the rounding of 3.12 to 3.00, the main difference between Equations 18b and 19 is that the AISC equation uses the total depth of the beam and column, whereas Equation 18b uses the effective depth.

THE REVISED KRAWINKLER MODEL

Due to the inability of many computer programs to model inelastic shear panels as used in the original Krawinkler model, the revised model shown in Figure 5 is often used. Here, the shear panel is represented by a single rotational spring, shown at the upper left of the model. All four flange springs are lumped into a single rotational spring, placed at the lower right. The remaining two corners act as zero-stiffness rotational hinges.

The properties of the panel spring, in terms of moment and rotation, are derived from the properties of the shear panel of the original model, which was in terms of shear force and shear strain. The rotational strength of the single panel spring is βH times the shear strength of the panel. Hence, using Equation 7 and multiplying by βH to convert shear to moment

$$\bar{M}_{PK} = V_{py}\beta H = 0.6F_y\alpha L\beta Ht_p = 0.6F_y\nabla_P \quad (20)$$

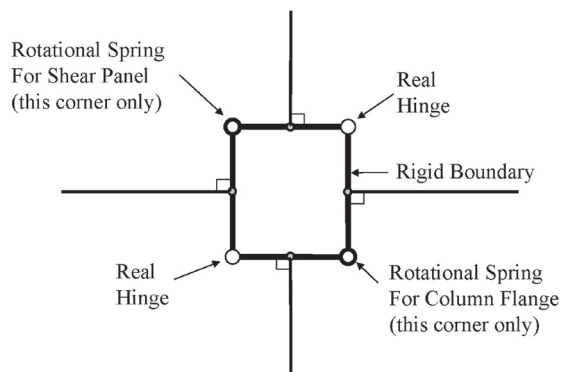


Fig. 5. The revised Krawinkler model.

where the new term, ∇_P , represents the effective volume of the panel zone. The bar over the M in Equation 20 designates that the property is intended for use in the modified Krawinkler model. Similar nomenclature is used for the remaining properties below.

Rotation in the panel spring in the modified model is synonymous with shear strain in the panel, thus the rotational stiffness of the panel spring can be computed as

$$\bar{K}_{PK} = \frac{\bar{M}_{PK}}{\theta_y} = \frac{0.6F_y\nabla_P}{\left(\frac{0.6F_y}{G}\right)} = G\nabla_P \quad (21)$$

The properties of the flange spring in the revised model are similar to those in the original model, except the revised model lumps all of the springs into one location. Hence, using Equations 10 and 16 and multiplying by 4,

$$\bar{K}_{FK} = 4K_{F0} = 4\frac{E(b_{fC})(t_{fC})^2}{10} = 1.04G(b_{fC})(t_{fC})^2 \quad (22)$$

$$\bar{M}_{FK} = 4M_{Fy} = 1.87F_y(b_{fC})(t_{fC})^2 \quad (23)$$

A summary of the properties of the Revised Krawinkler model (using the original force-deformation relationships of Figure 4) is presented in Table 2.

REVISED KRAWINKLER MODEL WITH REVISED FORCE-DEFORMATION BEHAVIOR

An alternative force-deformation relationship for the two components of joint behavior is shown in Figure 6. Here, the panel component of behavior is identical to that assumed by Krawinkler, but the flange component provides immediate resistance. Using the revised Krawinkler model, and assuming that the yield strength of the flange component is unchanged, the rotational stiffness of the flange component will reduce to

Table 3. Summary of Properties for Revised Krawinkler Model Using Revised Force-Deformation Relationships				
Component	Spring Type	No. of Springs	Spring Stiffness	Spring Strength
Panel	Rotational	1	$\tilde{K}_{FK} = G\nabla_P$	$\tilde{M}_{FK} = 0.6F_v\nabla_P$
Flanges	Rotational	1	$\tilde{K}_{FK} = 0.78G(b_{fC})(t_{fC})^2$	$\tilde{M}_{FK} = 1.87F_y(b_{fC})(t_{fC})^2$
See Figure 5 for illustration of model See Figure 6 for force-deformation relationships				

$$\tilde{K}_{FK} = \frac{3}{4}\bar{K}_{FK} = 0.78(b_{fC})(t_{fC})^2 G \quad (24)$$

where the tilde over the K term represents the fact that this is to be used in the revised Krawinkler model, using the revised constitutive properties. A summary of the required properties for the revised model using the revised force-deformation properties is provided in Table 3.

It is noted that the force-deformation behavior of the flanges of the column (and for that matter, of the panel) as described above is, in essence, empirical. In this sense, it is a viable mathematical model for an observed (and rather complex) physical behavior. Other models have been suggested to represent the same behavior. For example, Schneider and Amidi (1998) provide a more detailed model for the column flange component of behavior, Kim and Englehardt (1995) provide modifications to the effective depth terms, and Foutch and Yun (2002) describe complex hysteretic models for use in nonlinear response history analysis.

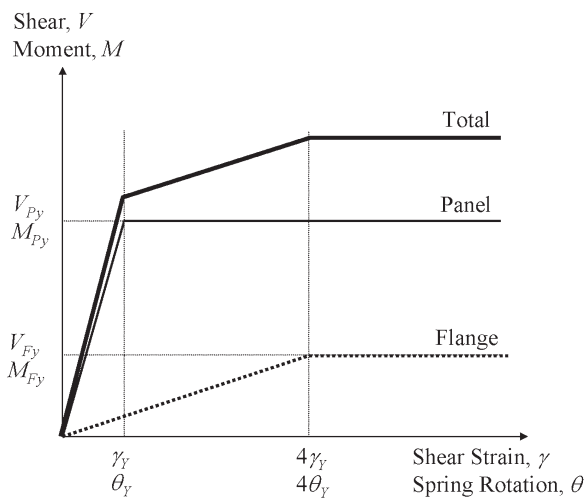


Fig. 6. Revised force-deformation/moment-rotation relationship.

As a final comment on the Krawinkler model, it is interesting to note that the properties for the flange spring are completely independent of those of the panel, even though the yield strain of the flange component is numerically tied to the shear stiffness of the panel. This independence is due to the fact that the yield strain in the panel is a function of only the shear modulus of the steel and the yield strength of the steel. This strain will not change if, for example, doubler plates are used as panel reinforcement.

THE SCISSORS MODEL

The Scissors model is shown in Figure 7. This model derives its name from the fact that the model acts as a pair of scissors with a single hinge in the center. It is important to note that the beam and column properties in the joint region are assumed to be completely rigid. Only two nodes and four degrees of freedom are required to model the joint if member rigid end zones are used for the column and beam regions inside the panel zone. Six nodes and 16° of freedom are required if separate rigid elements are utilized at the member ends.

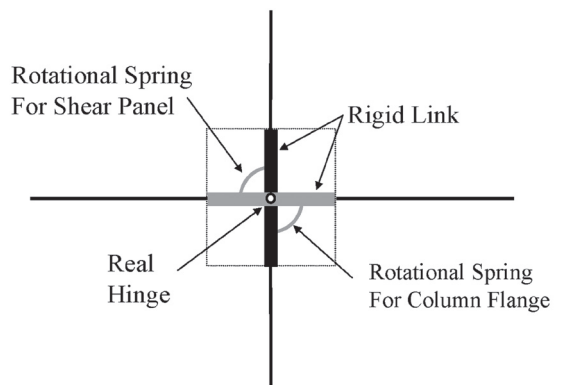


Fig. 7. The Scissors model.

As with the Krawinkler model, one rotational spring is used to represent the panel component and the other is used to represent the flange component of behavior. The properties of the Scissors model are determined in terms of those derived previously for the revised Krawinkler model, wherein a rotational spring is used to represent the panel component of strength and stiffness and a single rotational spring is used to represent the flange component of strength and stiffness. For the purpose of consistency in nomenclature, the revised moment-rotation relationship is used. Note, however, that this distinction is not necessary in the derivation.

The first step in the derivation is to determine the panel shear and the flange shear in the Krawinkler model in terms of the column shear. These shears are distributed in proportion to the rotational stiffness of the panel and flange springs as follows:

$$V_{P,K} = V_J \left(\frac{\tilde{K}_{PK}}{\tilde{K}_{PK} + \tilde{K}_{FK}} \right) = V_C \frac{(1-\alpha-\beta)}{\beta} \left(\frac{\tilde{K}_{PK}}{\tilde{K}_{PK} + \tilde{K}_{FK}} \right) \quad (25)$$

$$V_{F,K} = V_J \left(\frac{\tilde{K}_{FK}}{\tilde{K}_{PK} + \tilde{K}_{FK}} \right) = V_C \frac{(1-\alpha-\beta)}{\beta} \left(\frac{\tilde{K}_{FK}}{\tilde{K}_{PK} + \tilde{K}_{FK}} \right) \quad (26)$$

The next step is to determine the moments in the springs. These are simply βH times the shears:

$$M_{P,K} = V_{P,K} \beta H = V_C (1-\alpha-\beta) H \left(\frac{\tilde{K}_{PK}}{\tilde{K}_{PK} + \tilde{K}_{FK}} \right) \quad (27)$$

$$M_{F,K} = V_{F,K} \beta H = V_C (1-\alpha-\beta) H \left(\frac{\tilde{K}_{FK}}{\tilde{K}_{PK} + \tilde{K}_{FK}} \right) \quad (28)$$

The total drift over the height of the column can be found from virtual work. This is done by applying virtual unit shears in opposing directions at the top and the bottom of the column. Under this loading, the virtual moments are the same as given above, except 1.0 is substituted for V_C . The virtual quantities are shown with a carat in Equation 29, which equilibrates internal work and external work.

$$(1)\delta_K = \frac{M_{P,K} \hat{M}_{P,K}}{\tilde{K}_{PK}} + \frac{M_{F,K} \hat{M}_{F,K}}{\tilde{K}_{FK}} \quad (29)$$

The subscript K on the δ term in Equation 29 indicates that the drift is obtained from the Krawinkler model. After substitution and simplification, the resulting drift is

$$\delta_K = V_C \frac{(1-\alpha-\beta)^2 H^2}{\tilde{K}_{PK} + \tilde{K}_{FK}} \quad (30)$$

The drift in the Scissors model is found in a similar fashion. For an applied column shear V_C , the real moments in the scissors springs are

$$M_{P,S} = V_C H \left(\frac{\tilde{K}_{PS}}{\tilde{K}_{PS} + \tilde{K}_{FS}} \right) \quad (31)$$

$$M_{F,S} = V_C H \left(\frac{\tilde{K}_{FS}}{\tilde{K}_{PS} + \tilde{K}_{FS}} \right) \quad (32)$$

where \tilde{K}_{PS} and \tilde{K}_{FS} represent the rotational stiffness of the panel and flange springs, respectively. The virtual moments are the same as given by Equations 31 and 32, but a value of 1.0 replaces the column shear. Upon equating external and internal work,

$$(1)\delta_S = \frac{M_{P,S} \hat{M}_{P,S}}{\tilde{K}_{PS}} + \frac{M_{F,S} \hat{M}_{F,S}}{\tilde{K}_{FS}} \quad (33)$$

After substitution and simplification, the total drift obtained from the scissors model is

$$\delta_S = V_C \frac{H^2}{\tilde{K}_{PS} + \tilde{K}_{FS}} \quad (34)$$

As this displacement must be identical to that given in Equation 30, it is evident that the relationship between the Scissor spring stiffness and the Krawinkler spring stiffness is

$$\tilde{K}_{PS} + \tilde{K}_{FS} = \frac{\tilde{K}_{PK} + \tilde{K}_{FK}}{(1-\alpha-\beta)^2} \quad (35)$$

Using Equations 27 and 28 together with 31 and 32, a similar relationship exists between the Scissors and Krawinkler spring moments:

$$M_{P,S} + M_{F,S} = \frac{M_{P,K} + M_{F,K}}{(1-\alpha-\beta)} \quad (36)$$

Note, however, that the dimensionless quantity in the denominator is not squared.

Table 4. Summary of Properties for Scissors Model Using Revised Force-Deformation Relationships				
Component	Spring Type	No. of Springs	Spring Stiffness	Spring Strength
Panel	Rotational	1	$\tilde{K}_{PS} = \frac{G\nabla_P}{(1-\alpha-\beta)^2}$	$\tilde{M}_{PS} = \frac{0.6F_y\nabla_P}{(1-\alpha-\beta)}$
Flanges	Rotational	1	$\tilde{K}_{FS} = \frac{0.78G(b_{fC})(t_{fC})^2}{(1-\alpha-\beta)^2}$	$\tilde{M}_{FS} = \frac{1.87F_y(b_{fC})(t_{fC})^2}{(1-\alpha-\beta)}$
See Figure 7 for illustration of model See Figure 6 for force-deformation relationships				

Equation 35 is applicable when either the panel spring or the flange spring is zero. Hence, the general relationship between the spring stiffness in the Scissors and Krawinkler models is

$$K_s = \frac{K_k}{(1-\alpha-\beta)^2} \quad (37)$$

Similarly, the relationship between the corresponding moments, including the yield moments, is

$$M_s = \frac{M_k}{(1-\alpha-\beta)} \quad (38)$$

The properties required for modeling the panel as a scissor joint are summarized in terms of the physical joint properties in Table 4.

One should note from Tables 3 and 4 that while the properties of the Scissors model are dependent on the quantities α and β , those of the Krawinkler model are not. Since it was explicitly assumed that the columns and beams on both sides

of the joint are of equal height and span, and these terms are reflected in α and β , the equations shown in Table 4 should not be used for interior joints when this condition is violated. There is no such restriction for exterior joints.

COMPARISONS BETWEEN THE KRAWINKLER AND SCISSORS MODELS

In the first part of this paper, the properties of the Scissors model were derived to provide identical force-deformation relationships for subassemblages that are analyzed using the Krawinkler model. The strength and stiffness properties derived for the springs in the two models are different because the rotations in the Krawinkler springs are $1/(1-\alpha-\beta)$ times larger than the rotations in the Scissors springs when the total subassemblage drift is identical.

The difference in rotations is apparent in the deflected shapes shown in Figure 8a and 8b. In this figure all of the deformation is assumed to be in the panel, with the beam and column rigid. It is very important to note, however, that it is not only the spring rotations that are different. In fact, the entire kinematic behavior is different. One of the more

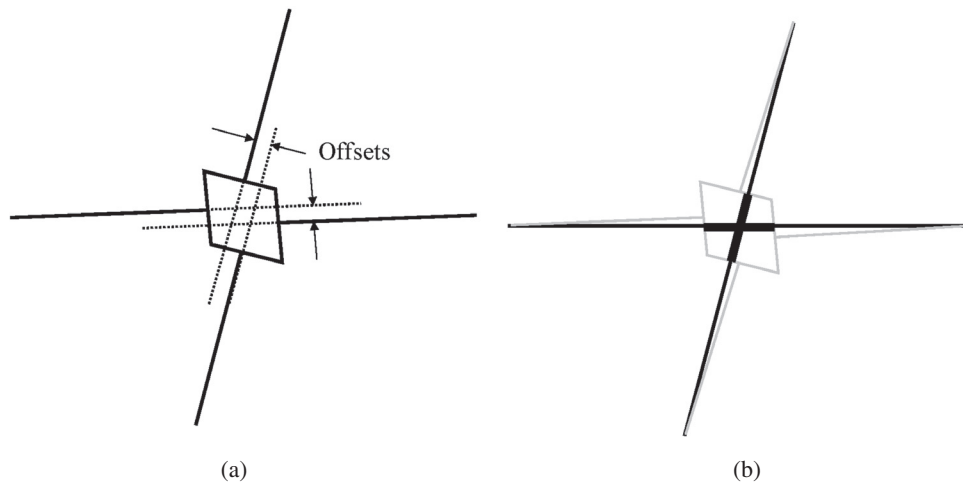


Fig. 8. Kinematics of Krawinkler model (a) and Scissors model (b).

Table 5a. Computed Properties for the Krawinkler Model (Weak Panel)					
Column	Beam	\tilde{K}_{PK} (kN-m/rad)	\tilde{M}_{PK} (kN-m)	\tilde{K}_{FK} (kN-m/rad)	\tilde{M}_{FK} (kN-m)
W530×182	W610×125	3.66×10^5	9.84×10^2	1.12×10^4	1.21×10^2
W530×219	W690×140	4.97×10^5	1.33×10^3	1.63×10^4	1.75×10^2
W530×300	W690×140	6.41×10^5	1.73×10^3	3.29×10^4	3.54×10^2

Table 5b. Computed Properties for the Krawinkler Model (Strong Panel)					
Column (Doubler, mm)	Beam	\tilde{K}_{PK} (kN-m/rad)	\tilde{M}_{PK} (kN-m)	\tilde{K}_{FK} (kN-m/rad)	\tilde{M}_{FK} (kN-m)
W530×182 (25.4)	W610×125	9.76×10^5	2.62×10^3	1.12×10^4	1.21×10^2
W530×219 (25.4)	W690×140	1.19×10^6	3.20×10^3	1.63×10^4	1.75×10^2
W530×300 (22.2)	W690×140	1.25×10^6	3.38×10^3	3.29×10^4	3.54×10^2

Table 6a. Computed Properties for the Scissors Model (Weak Panel)					
Column	Beam	\tilde{K}_{PS} (kN-m/rad)	\tilde{M}_{PS} (kN-m)	\tilde{K}_{FS} (kN-m/rad)	\tilde{M}_{FS} (kN-m)
W530×182	W610×125	5.98×10^5	1.25×10^3	1.83×10^4	1.55×10^2
W530×219	W690×140	8.53×10^5	1.75×10^3	2.79×10^4	2.29×10^2
W530×300	W690×140	1.10×10^6	2.26×10^3	5.67×10^4	4.64×10^2

striking differences is the presence of offsets in the center-lines of the columns and beams in the Krawinkler model, which are not present in the Scissors model. A related difference is the rotations at the ends of the beams and columns.

The kinematic differences lead to questions as to how the models perform in full structures. In particular, will a pushover curve (or a response history trace) developed for a full structure using the Krawinkler model be the same as that for the same full structure using the Scissors model? Further, how do the presence of beam hinging, gravity load, and the inclusion of P-Delta affect the full structure response?

To answer these questions, an extensive series of analyses were carried out using DRAIN-2DX (Prakash and Powell, 1993). The structure analyzed was a six-story moment resisting frame. An elevation of the frame is shown in Figure 9. Two variations of this structure were analyzed, a weak panel version and a strong panel version. The computed properties for the various panels are presented in Tables 5 and 6. Note that all values are based on $E = 200$ GPa (29,000 ksi),

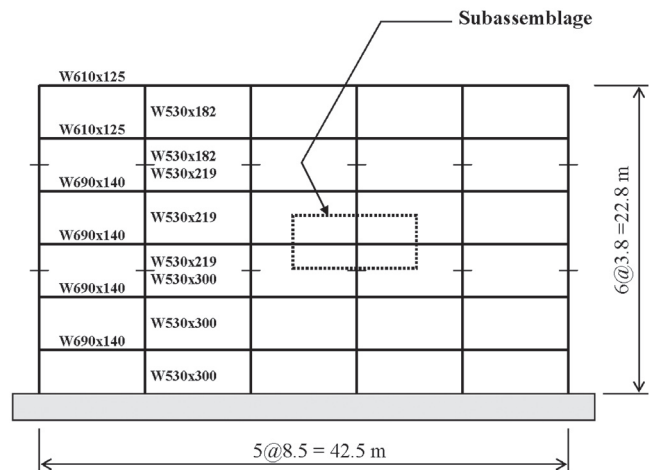


Fig. 9. Frame analyzed for comparison of Krawinkler and Scissors models.

Column (Doubler, mm)	Beam	\tilde{K}_{PS} (kN-m/rad)	\tilde{M}_{PS} (kN-m)	\tilde{K}_{FS} (kN-m/rad)	\tilde{M}_{FS} (kN-m)
W530×182 (25.4)	W610×125	1.59×10^6	3.36×10^3	1.83×10^4	1.55×10^2
W530×219 (25.4)	W690×140	2.03×10^6	4.18×10^3	2.79×10^4	2.29×10^2
W530×300 (22.2)	W690×140	2.17×10^6	4.44×10^3	5.67×10^4	4.64×10^2

U.S. column designations: W21×122 (1 in.), W21×147 (1 in.), and W21×201 (7/8 in.)
U.S. beam designations: W24×84 and W27×94

Beam	K1 (kN-m/rad)	M1 (kN-m)	K2 (kN-m/rad)	M2 (kN-m)	K3 (kN-m/rad)
W610×125	1.13×10^9	1.25×10^3	3.68×10^4	1.38×10^3	1.05×10^4
W690×140	1.13×10^9	1.53×10^3	5.09×10^4	1.70×10^3	1.50×10^4

Run	Model	Girder Yielding	See Figure No.
S1a	K	N	10
S1b	S	N	
S1c	S/K	N	
S2a	K	Y	11
S2b	S	Y	
S2c	S/K	Y	

$G = 77$ GPa (11,150 ksi) and $F_y = 345$ MPa (50 ksi). Doubler plate thicknesses for the strong panel model are shown in the first column of Tables 5b and 6b. A strain hardening value of 3% of the initial elastic stiffness was used for the beams outside the panel zone. Strain hardening of 1% was used in the panel zone regions.

Yielding for the beams was provided by tri-linear rotational springs. The computed properties for these springs are shown in Table 7. Details for determining beam properties are not provided herein but are discussed in the second part of the Structural Analysis example in the *Guide to the Application of the 2003 NEHRP Recommended Provisions in Earthquake-Resistant Design* (FEMA, 2005). Columns were designed using a strong column weak beam philosophy, and were not allowed to yield during the analysis.

For the purpose of brevity, only the results for the weak panel structures are presented in detail. The behavior exhibited by the strong panel models is discussed only in relation to the behavior of the weak panel models.

The first set of analyses consisted of pushover analysis of a single interior subassemblage with a W690×140 (W27×94) girder and W530×300 (W21×201) column. A summary of the analysis parameters is shown in Table 8. In the table “K” represents the Krawinkler model, “S” is the Scissors model, and “S/K” is the Scissors model with Krawinkler properties. Girder yielding is indicated as “N” for not included, and “Y” for included.

It is very important to note that the S/K model is theoretically incorrect. It is used only to illustrate the effect of using the properties derived for the Krawinkler model in the Scissors model.

The results for the subassembly analysis are shown in Figures 10 and 11. These plots are presented in a dimensionless form, where the horizontal axis quantifies the total subassembly drift divided by the subassembly height, and the vertical axis represents the column shear divided by the maximum applied shear.

As shown in Figure 10, which is for the analysis without girder yielding, the responses for the Krawinkler model and the Scissors model are identical. This is expected because the Scissors model properties were derived to produce deformations consistent with the Krawinkler model. The curve for the Scissors model with the Krawinkler spring properties indicates a response that has significantly less strength and stiffness than the true behavior. This is also as expected because the stiffness and strength of the rotational springs for the Krawinkler model are less than those for the Scissors model by the factors $(1 - \alpha - \beta)^2$ and $(1 - \alpha - \beta)$, respectively.

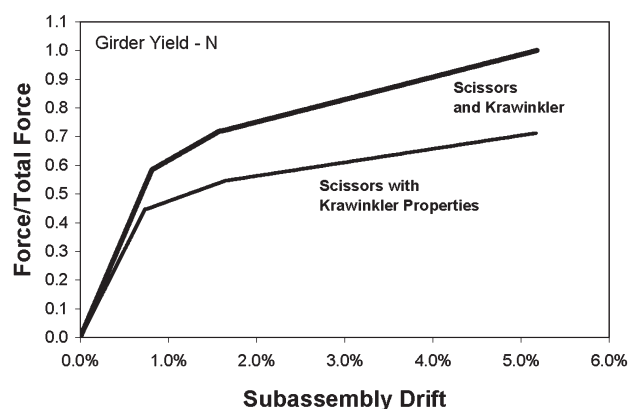


Fig. 10. Results for subassembly analysis (models S1a-S1c).

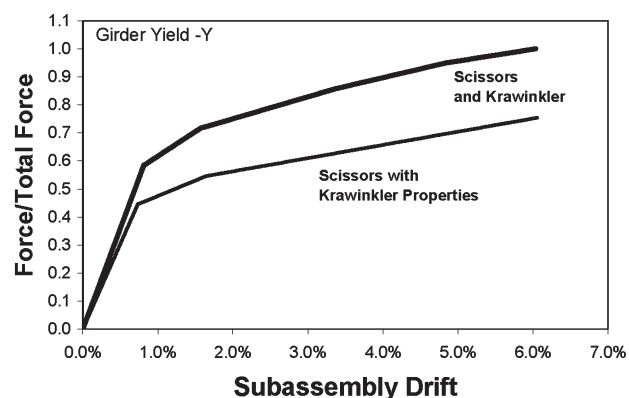


Fig. 11. Results for subassembly analysis (models S2a-S2c).

In Figure 10, it is noted that the difference between the strengths represented by the upper and lower curves is directly related to the quantity $(1 - \alpha - \beta)$, but the apparent difference in the stiffness, represented by initial the slopes of the curves, is much less than would be expected from $(1 - \alpha - \beta)^2$. The reason for this is that the panel zone deformations contribute only a portion of the total subassembly flexibility (the other components being due to flexural and shear deformations in the beams and columns).

The computed responses for the subassembly with girder yielding invoked is shown in Figure 11. Again the curves for the Krawinkler and Scissors models are identical, even at drifts beyond girder yielding (which occurs, due to the weak panel, at a drift of about 5%). As before, the S/K model produces results that indicate a significant reduction in strength and stiffness. Girder yielding did occur in the S/K model, but at drifts well beyond those shown in the plot.

The second set of analyses was nonlinear pushover analysis of the full six-story structure. The various parameters are listed in Table 9. The column of the table headed “Continuity” represents whether or not the columns and the beams were continuous in the structure. The indicator “D,” for discontinuous, means that the columns and the beams had zero-stiffness rotational hinges placed at mid-height and mid-span, respectively. When these hinges are active the structure behaves as an assemblage of subassemblies. When the hinges are removed (indicator “C” in Table 9) the structure acts as a fully continuous moment resisting frame. The other parameters that were considered in the analysis were girder yielding, the presence of gravity load, and whether or not P-Delta effects were included. These are all Y/N parameters in Table 9.

The results from the nonlinear static pushover of the full moment frames are presented in Figures 12 through 17. In each of these figures the vertical axis is the resisting shear

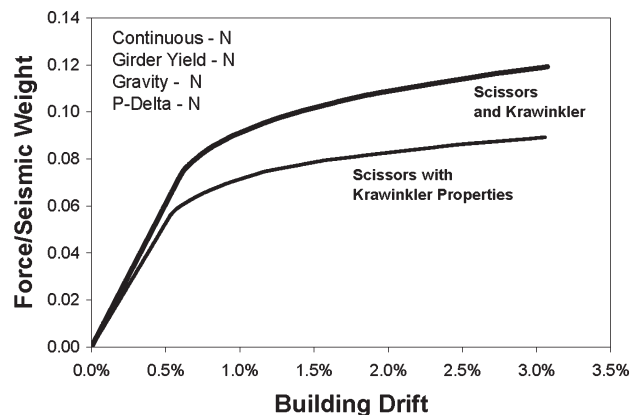


Fig. 12. Static pushover results for full structure (models F1a-F1c).

Table 9. Analysis Parameters for Full Structure Pushover Analysis						
Run	Model	Girder Yielding	Continuity	Gravity Load	P-Delta	See Figure
F1a	K	N	D	N	N	12
F1b	S	N	D	N	N	
F1c	S/K	N	D	N	N	
F2a	K	Y	D	N	N	13
F2b	S	Y	D	N	N	
F2c	S/K	Y	D	N	N	
F3a	K	N	C	N	N	14
F3b	S	N	C	N	N	
F3c	S/K	N	C	N	N	
F4a	K	Y	C	N	N	15
F4b	S	Y	C	N	N	
F4c	S/K	Y	C	N	N	
F5a	K	Y	C	Y	N	16
F5b	S	Y	C	Y	N	
F5c	S/K	Y	C	Y	N	
F6a	K	Y	C	Y	Y	17
F6b	S	Y	C	Y	Y	
F6c	S/K	Y	C	Y	Y	

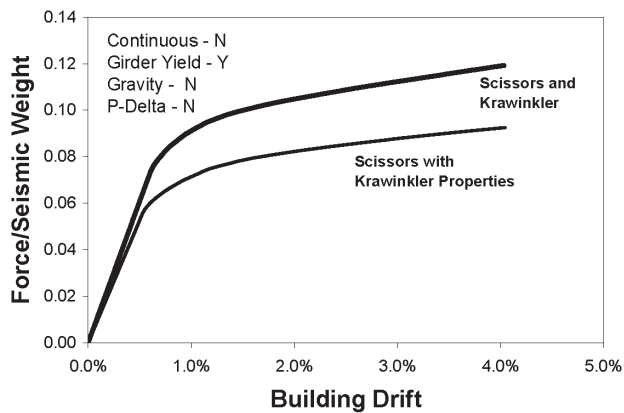


Fig. 13. Static pushover results for full structure (models F2a–F2c).

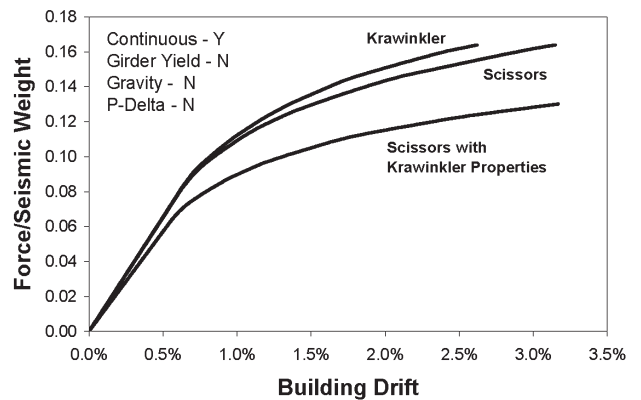


Fig. 14. Static pushover results for full structure (models F3a–F3c)

divided by the building weight tributary to the frame, and the horizontal axis is the total roof drift divided by the total building height. From Figures 12 and 13 it can be seen that regardless of the presence of girder yielding, the Krawinkler and Scissors models produce exactly the same results when the beams and columns have mid-span and mid-height hinges. This is due to the fact that when the inflection points are forced to be at mid-span and mid-height, the structure behaves as an assemblage of subassemblages. The properties for these subassemblages were derived to produce identical displacement responses. As with the individual subassemblages, it is evident from the pushover curves that the use of the Krawinkler spring properties in the Scissors model produces a significant reduction in both strength and initial stiffness of the structure.

The pushover curves of Figures 14 and 15 are based on the same models as those shown in Figures 12 and 13, except that the beams and columns are continuous. As may be

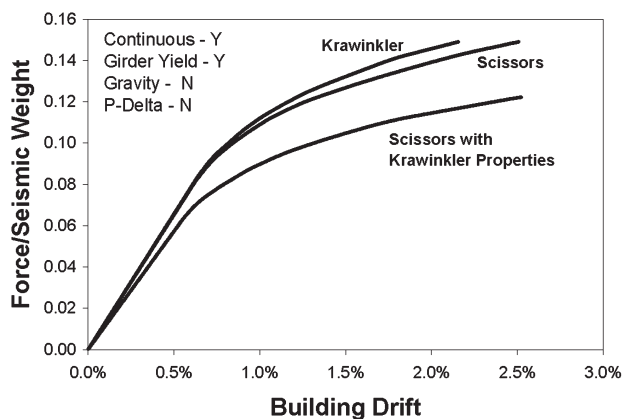


Fig. 15. Static pushover results for full structure (models F4a-F4c).

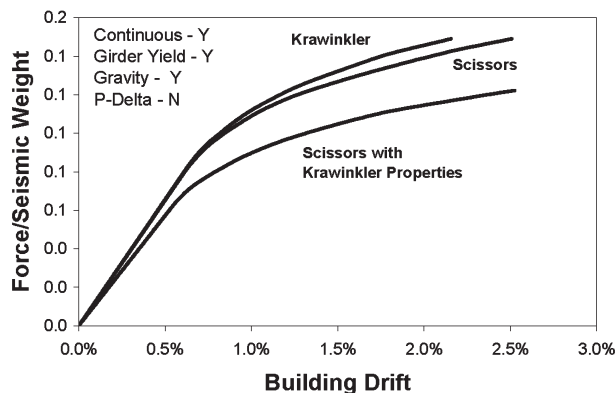


Fig. 16. Static pushover results for full structure (models F5a-F5c).

observed from the figures, the curves for the Krawinkler and Scissors model are no longer identical. The divergence of the two curves is particularly pronounced after first yield. The reason for the divergence is that the inflection points for the continuous model are no longer at mid-height and mid-span of the columns and girders, respectively. The curve for the Krawinkler model is theoretically correct because the properties for the Krawinkler springs depend only on the panel zone properties. The response curve for the Scissors model, although close to that of the Krawinkler, is incorrect because the terms α and β are effectively a function of the location of the inflection points, and these inflection points move as the yielding in the structure progresses.

The lower curves in Figures 14 and 15 are for the structure modeled with Scissors joint, but using the Krawinkler properties. Again, the stiffness and strength is very significantly underestimated.

The addition of gravity load to the continuous model does not cause a significant increase in the variance in the results, as is shown in Figures 15 and 16. P-Delta effects were not included in the analysis that generated the curves shown in Figure 16, but these effects were included in the analysis that produced Figure 17. The only significant difference with the addition of gravity load is the order (sequence) of girder yielding due to the pre-imposed gravity load moments. As expected, the inclusion of P-Delta effects causes additional drift. A greater discrepancy between the Krawinkler and Scissors model results is also evident. The final difference in drift between the two models with gravity only is approximately 14% (see Figure 16). After the addition of P-Delta effects, the drift in the Scissors model increases to be over 30% greater than the Krawinkler (see Figure 17). However, it should be noted that the overall post-yield drift also doubles due to the P-Delta effect.

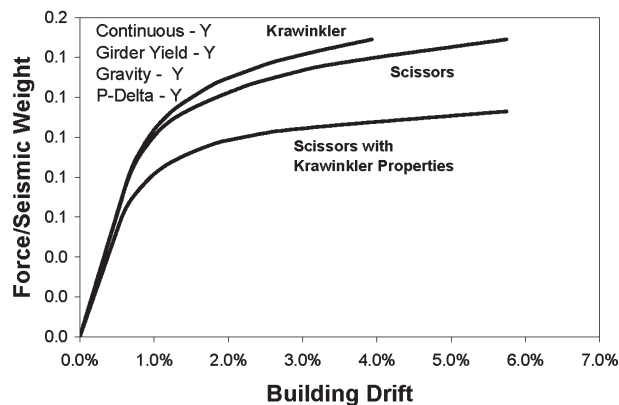


Fig. 17. Static pushover results for full structure (models F6a-F6c).

Table 10. Analysis Parameters for Full Structure Response History and IDA Analysis						
Run	Model	Girder Yielding	Continuity	Gravity Load	P-Delta	See Figure
R1a	K	Y	C	Y	N	18, 20
R1b	S	Y	C	Y	N	
R1c	S/K	Y	C	Y	N	
R2a	K	Y	C	Y	Y	19, 21
R2b	S	Y	C	Y	Y	
R2c	S/K	Y	C	Y	Y	

The S/K model results for the full structures are also plotted in Figures 16 and 17. As before, the behavior of the structures with the Krawinkler properties in the Scissors model shows a marked reduction in strength and stiffness.

A set of pushover curves similar to those shown in Figures 10 through 17 were also produced for the structure with strengthened panel zones in all interior joints. The same trends as observed for the weak panel models were evident, but there was less difference in the behavior of the Krawinkler and Scissors models because the dominant source of yielding shifted to the girder hinges.

The final set of analyses performed were nonlinear response history analyses for the structure subjected to the Northridge earthquake. Single response histories were performed, as were Incremental Dynamic Analyses (IDA) (Vamvatsikos, 2002). The response histories and IDA were run using the Northridge earthquake acceleration record from the Sylmar County Hospital. The record was scaled to provide a seismic coefficient, C_s , of 0.27 at the first vibration mode of the structure. Damping of approximately 5% critical was assumed in the analysis. Damping was provided with a special “outrigger” frame to avoid problems

associated with the use of stiffness proportional damping in yielding elements.

The IDA intensity factor started at 0.2 times the scaled earthquake record and stepped up in increments of 0.2 to a final intensity factor of 2.0. The reported IDA damage index is the maximum roof drift ratio. The model parameters that were varied in both the response history and IDA analyses are provided in Table 10.

The response history plots are shown in Figures 18 and 19. In each case the beams and columns were fully continuous, the girders were allowed to yield, and gravity load was present. In the analysis represented in Figure 18, P-Delta effects were ignored, but these effects are included in the analysis that generated the curves of Figure 19.

As shown in Figure 18, the Krawinkler and Scissors models produce nearly identical roof drift response, with a few visible differences in the curves. The addition of P-Delta effects produced a more visible difference between the Krawinkler and Scissors models in both the maximum response and in the residual displacement (see Figure 19). This change corresponds to the same widened gap as was seen with the static pushover curves due to P-Delta effects.

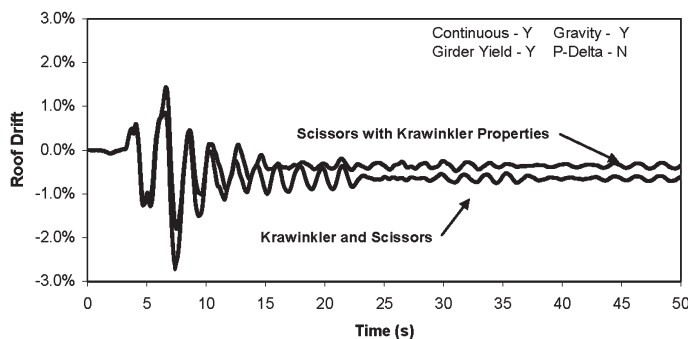


Fig. 18. Response history results for full structure (models R1a–R1c).

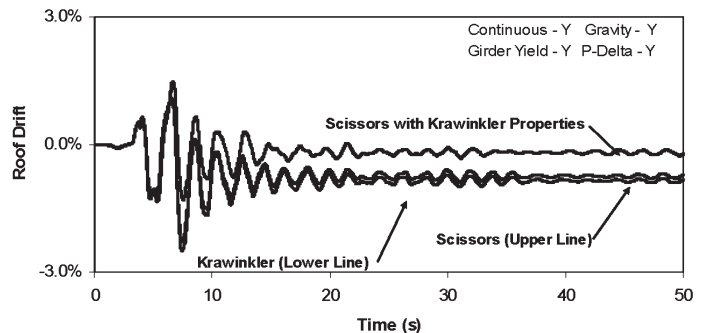


Fig. 19. Response history results for full structure (models R2a–R2c).

SUMMARY AND CONCLUSIONS

It is also interesting to note that while static analyses indicated that the S/K model was consistently weaker and more flexible than the Krawinkler or Scissors Model, the response history shows a reduction in both maximum drift and residual displacement for this model. This might imply a *stiffer* S/K model. However, this judgement is inappropriate because the displacement history trace is highly influenced by continuously changing structural properties. Different observations regarding the relative behaviors of the various models may be evident when the ground motion is scaled up or down.

In the Incremental Dynamic Analysis, the ground motions are scaled up or down as indicated in the previous paragraph. The resulting IDA curves are shown in Figures 20 and 21. The curves in Figure 20 were generated for the model with full continuity, girder yielding, and gravity load, but without P-Delta. P-Delta effects were included for the analysis that generated Figure 21.

From Figure 20, it is noted that for all the runs up to an intensity factor of 0.6 the Krawinkler and Scissors models are in very reasonable agreement. A greater flexibility is apparent in the S/K model. At an intensity factor of about 0.8, the Scissors and Krawinkler models still match well but the S/K model has diverged on the low side and has actually begun a “resurrection.” Above an intensity factor of 1.0 each model has moved to its own path. While the Scissors and Krawinkler models are still behaving somewhat similarly, the S/K is more quickly moving toward failure. The same type of trends can be seen in Figure 21, where the IDA curves were generated for the structures with P-Delta effects included. The S/K model’s movement toward failure is more evident with P-Delta. The performance of the Krawinkler and Scissors model in the IDA shows that the dynamic behavior of the two models differs especially as the nonlinearity increases and more deformation is required of the panel zone.

In the first part of this paper, spring properties were derived for both the Krawinkler and Scissors models of beam-column joints. During the derivation, it was shown that under a given subassembly drift, the rotations in the springs of the two models are not the same. This discrepancy is due to differences in the kinematic behavior of the models.

As a result of the differing behavior, the derived properties for the springs in the Krawinkler and Scissors models are not the same. This finding contradicts the *incorrect* recommendation of several published documents, including FEMA 355F, that indicate that the properties derived for the Krawinkler model may be used in the Scissors model.

Using the Krawinkler and Scissors spring properties derived in this paper, it was shown that identical nonlinear static pushover behavior is predicted for simple subassemblages, modeled with and without girder hinging. Larger structures that are modeled as an assemblage of subassemblages also have identical pushover behavior.

When fully continuous models are analyzed, differences in pushover curves developed from the Krawinkler and Scissors models become evident. These differences are due to shifting inflection points. The shifting inflection points affect only the Scissors model, because the properties for this model were derived based on the assumption that the inflection points are at midheight of the columns and midspan of the girders.

When the properties derived for the Krawinkler model are used in a Scissors model, the predicted strength and stiffness from the pushover analysis is significantly less than that of the true system. This error, if continued in practice, will have a negative effect on the economy of moment resisting steel frame structures.

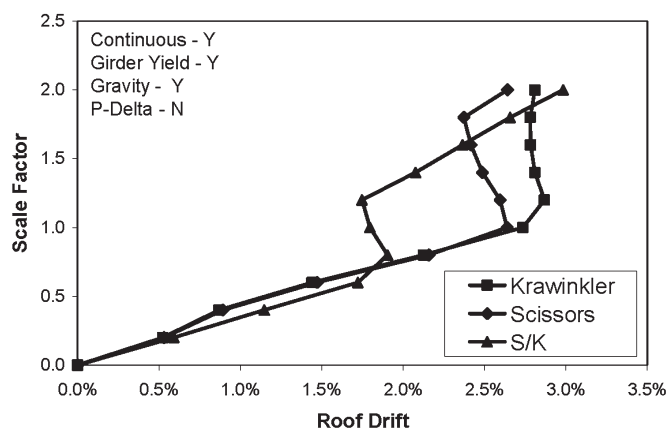


Fig. 20. IDA results for full structure (models R1a-R1c).

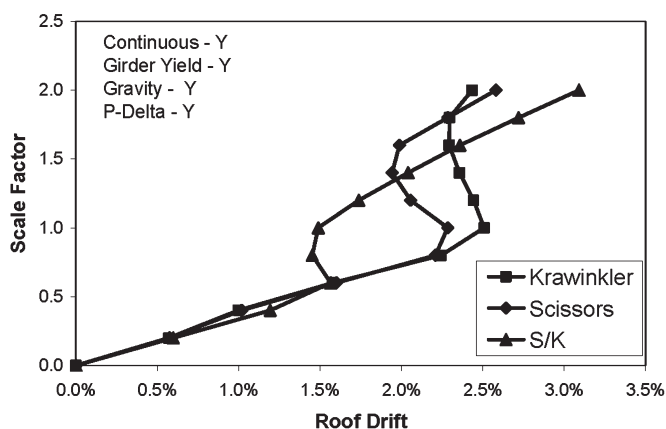


Fig. 21. IDA results for full structure (models R2a-R2c).

When nonlinear response history analysis is performed, the Krawinkler and Scissors models produce similar behaviors under low-intensity ground motion, but very significant differences in behavior become evident under larger ground motions.

When response history analysis is performed on structures with Krawinkler spring properties inserted into the Scissors models, the predicted displacements may be more or less than those predicted using the appropriate models. For the ground motion used in the analysis, it appeared that the structure with the improper Scissors model was moving toward collapse at a much more rapid rate than for the structure that is modeled properly. This is likely due to the fact that the improper model significantly underestimates the static strength of the structure.

Recommendations

On the basis of the above findings, the following recommendations are provided:

1. Never use a Scissors model with spring properties that have been derived for the Krawinkler model.
2. Even though it is more complex, the Krawinkler model is preferred over the Scissors model. This is because the kinematic behavior of the Krawinkler model is much more representative of the true behavior of the joint than is the Scissors model. Furthermore, the properties for the Krawinkler model depend only on the properties of the beam-column joint, whereas the properties of the Scissors model are also a function of the lengths of the columns and beams.
3. The higher the ductility demand, the larger discrepancy between the Scissors and the Krawinkler model. Therefore, the Scissors model is appropriate only for elastic structures or for systems where ductility demands are low.

Limitations of the Study and Needs for Future Research

In this study reported herein, flexural deformations were not included in the beam-column joint region. Models that include such deformation have been suggested by several researchers [for example, Downs (2002)]. However, there is considerable uncertainty with regard to the true flexural behavior in the beam-column joint region, and these uncertainties make it difficult to validate the derived models.

Additionally, all the analysis on which these findings were based was performed for strong column systems. Systems with yielding columns should also be analyzed, as it is expected that larger differences between results generated by the Krawinkler and Scissors models may be encountered for these structures when ductility demands are high. It is

not expected, however, that inclusion of column yielding will significantly alter the principal recommendations listed above.

ACKNOWLEDGMENTS

The authors would like to acknowledge the efforts of graduate student Rakesh Pathak and Professor Sam Easterling, both of Virginia Tech, who reviewed the manuscript of this paper prior to submittal. Part of the junior author's graduate stipend was provided by the Charles E. Via Fellowship endowment for the Virginia Tech Department of Civil and Environmental Engineering.

NOMENCLATURE

α	Ratio of effective depth of column to span length
β	Ratio of effective depth of beam to column height
γ_y	Shear strain at yield
δ_K	Drift obtained from Krawinkler model
δ_S	Drift obtained from Scissors model
Δ	Lateral displacement over height H
Δ_C	Column contribution to displacement Δ
Δ_B	Beam contribution to displacement Δ
Δ_J	Beam-column joint contribution to displacement Δ
Δ_{JA}	Axial contribution to Δ_J
Δ_{JF}	Flexural contribution to Δ_J
Δ_{JV}	Shear contribution to Δ_J
b_{fC}	Width of column flange
d_C	Total depth of column
d_B	Total depth of beam
t_P	Panel zone thickness, equal to column web thickness + doubler plate thickness
t_{fC}	Thickness of column flange
t_{fB}	Thickness of beam flange
C_S	Seismic response coefficient
E	Modulus of elasticity of steel
F_y	Yield stress of steel used in column and doubler plate
G	Shear modulus of steel
H	Height of column from center of story above to center of story below
L	Length of beam from center of bay to center of bay

K_K	Stiffness of Krawinkler model spring	\tilde{M}_{FK}	Flange component yield strength for revised Krawinkler model with revised force-deformation relationship
K_S	Stiffness of Scissors model spring	\tilde{M}_{PS}	Panel zone component yield strength for Scissors model
$K_{P\gamma}$	Panel zone component shear stiffness	\tilde{M}_{FS}	Flange component yield strength for Scissors model
$K_{F\gamma}$	Column flange component shear stiffness	M_{FK}	Moment in Krawinkler spring due to column flange bending resistance
$K_{F\theta}$	Column flange component rotational spring stiffness	M_{PK}	Moment in Krawinkler spring due to panel shear resistance
K_{PK}	Panel zone component shear stiffness for original Krawinkler model	M_{FS}	Moment in Scissors spring due to column flange bending resistance
K_{FK}	Flange component spring stiffness for original Krawinkler model	M_{PS}	Moment in Scissors spring due to panel shear resistance
\bar{K}_{PK}	Panel zone component spring stiffness for revised Krawinkler model	R_V	Shear yield strength of beam-column joint per AISC <i>Specification</i>
\bar{K}_{FK}	Flange component spring stiffness for revised Krawinkler model	V_C	Average shear force in columns above and below the joint
\tilde{K}_{PK}	Panel zone component spring stiffness for revised Krawinkler model with revised force-deformation relationship	V_F	Column flange component of beam-column joint shear
\tilde{K}_{FK}	Flange component spring stiffness for revised Krawinkler model with revised force-deformation relationship	V_J	Horizontal shear force in beam-column joint
\tilde{K}_{PS}	Panel zone component spring stiffness for Scissors model	V_{JY}	Shear yield strength of beam-column joint
\tilde{K}_{FS}	Flange component spring stiffness for revised Scissors model	V_P	Panel zone component of beam-column joint shear
M_K	Moment in Krawinkler model spring	V_{Fu}	Column flange component ultimate shear force from virtual work
M_S	Moment in Scissors model spring	V_{FY}	Column flange component yield force
M_F	Moment in column flange component	V_{PY}	Panel zone component yield strength for original Krawinkler model
M_{FY}	Flange component yield moment	V_{FK}	Shear in Krawinkler spring due to column flange bending resistance
M_{FK}	Flange component yield strength for original Krawinkler model	V_{PK}	Shear in Krawinkler spring due to panel shear resistance
\bar{M}_{PK}	Panel zone component yield strength for revised Krawinkler model	V_{PK}	Flange component yield strength for original Krawinkler model
\bar{M}_{FK}	Flange component yield strength for revised Krawinkler model	∇_P	Volume of panel zone = $\alpha L\beta H t_p$
\tilde{M}_{PK}	Panel zone component yield strength for revised Krawinkler model with revised force-deformation relationship		

REFERENCES

- AISC (2005), *Specification for Structural Steel Buildings*, ANSI/AISC 360-05, March 9, American Institute of Steel Construction, Inc., Chicago, IL.
- AISC (2005), *Seismic Provisions for Structural Steel Buildings*, ANSI/AISC 341-05, March 9, American Institute of Steel Construction, Inc., Chicago, IL.
- ASCE (2002), *Minimum Design Loads for Buildings and Other Structures*, ASCE 7, American Society of Civil Engineers, Reston, VA.
- Becker, R., (1975), "Panel Zone Effect on the Strength and Stiffness of Steel Rigid Frames," *Engineering Journal*, American Institute of Steel Construction, Vol. 12, No.1, pp. 19–29.
- Bathe, K. (1996), *Finite Element Procedures*, Prentice Hall, Englewood Cliffs, NJ.
- Bertero, V.V., Popov, E.P., and Krawinkler, H. (1972), "Beam-Column Subassemblages Under Repeated Load," *Journal of the Structural Division*, ASCE, Vol. 98, No. ST5, pp. 1137–1159.
- Castro, J.M., Elghazouli, A.Y., and Izzuddin, B.A. (2005), "Modeling of the Panel Zone in Steel and Composite Moment Frames," *Engineering Structures*, Vol. 27, pp. 129–144.
- Charney, F.A. (1990), "Sources of Elastic Deformation in Laterally Loaded Steel Frame and Tube Structures," *Proceedings of the Fourth World Congress on Tall Buildings*, Council on Tall Buildings and Urban Habitat, Bethlehem, PA, pp. 893–915.
- Charney, F.A. (1993), "Economy of Steel Frame Buildings through Identification of Structural Behavior," *Proceedings of the Spring 1993 AISC Steel Construction Conference*, Orlando, Florida, pp. 12-1–12-33.
- Downs, W.M. (2002), *Modeling and Behavior of the Beam/Column Joint Region of Steel Moment Resisting Frames*, M.S. Thesis, Department of Civil and Environmental Engineering, Virginia Tech, Blacksburg, VA.
- FEMA (2000), *Recommended Seismic Design Criteria for New Steel Moment Frame Buildings*, FEMA 350, Federal Emergency Management Agency, Washington, DC.
- FEMA (2000a), *State of the Art on Systems Performance of Steel Moment Frames Subjected to Earthquake Ground Shaking*, FEMA 355C, Federal Emergency Management Agency, Washington, DC.
- FEMA (2000b), *State of the Art Report on Performance Prediction of Steel Moment Frames Subjected to Ground Shaking*, FEMA 355F, Federal Emergency Management Agency, Washington, DC.
- FEMA (2000c), *Prestandard and Commentary for the Seismic Rehabilitation of Buildings*, FEMA 356, Federal Emergency Management Agency, Washington, DC.
- FEMA (2004), *NEHRP Recommended Provisions for Seismic Regulations for New Buildings and Other Structures*, FEMA 450, Federal Emergency Management Agency, Washington, DC.
- FEMA (2005), *Guide to Application of the 2003 NEHRP Recommended Provisions in Earthquake-Resistant Design*, Federal Emergency Management Agency, Washington, DC.
- Foutch, D.A. and Yun, S. (2002), "Modeling of Steel Moment Frames for Seismic Loads," *Journal of Constructional Steel Research*, Vol. 58.
- Hibbit, Karlson, and Sorensen (2001), *ABAQUS User's Manual*, Version 6.2.
- Kim, K. and Engelhardt, M. (1995), *Development of Analytical Models for Earthquake Analysis of Steel Moment Frames*, Phil. M. Ferguson Structural Engineering Lab Report 95-2, University of Texas, Austin, TX.
- Krawinkler, H. (1978), "Shear in Beam-Column Joints in Seismic Design of Frames," *Engineering Journal*, American Institute of Steel Construction, Inc., Chicago, IL, Vol. 15, No. 3, pp. 82–91.
- Prakesh, V. and Powell, G.H. (1993), *DRAIN 2D-X Users Guide*, University of California, Berkeley, CA.
- Schneider, S.P. and Amidi, A. (1998), "Seismic Behavior of Steel Frames with Deformable Panel Zones," *Journal of Structural Engineering*, Vol. 124, No 1, pp. 35–42.
- Vamvatsikos, D. (2002), "Seismic Performance, Capacity, and Reliability of Structures as Seen Through Incremental Dynamic Analysis," Ph.D. Dissertation, Department of Civil and Environmental Engineering, Stanford University, Palo Alto, CA.